Sound production due to swirl–nozzle interaction
Model-based analysis of experiments

Hirschberg, L.; Hulshoff, S. J.; Bake, F.

DOI
10.2514/1.J059669

Publication date
2021

Document Version
Final published version

Published in
AIAA Journal

AIAA JOURNAL
Vol. 59, No. 4, April 2021

Sound Production due to Swirl–Nozzle Interaction: Model-Based Analysis of Experiments

L. Hirschberg*
DLR, German Aerospace Center, 10623 Berlin, Germany
S. J. Hulshoff†
Delft University of Technology, 2629 HS Delft, The Netherlands
and
F. Bake‡
DLR, German Aerospace Center, 10623 Berlin, Germany

https://doi.org/10.2514/1.J059669

Indirect noise due to the interaction of flow inhomogeneities with a choked nozzle is an important cause of combustion instability in solid rocket motors and is believed to be important in aircraft engines. A previously published experiment (Kings, N., and Bake, F., "Indirect Combustion Noise: Noise Generation by Accelerated Vorticity in a Nozzle Flow," *International Journal of Spray and Combustion Dynamics*, Vol. 2, No. 3, 2010, pp. 253–266.) demonstrated that interaction of a nozzle with time-dependent axial swirl can also be a source of sound. This axial swirl was generated by intermittent tangential mass injection upstream from a choked nozzle in a so-called vortex wave generator. The present work discusses the impact of swirl–nozzle interaction in this experiment on the acoustic waves detected downstream of the nozzle. The main source of sound appears to be the reduction in mass flux through the choked nozzle, which depends quadratically on the swirl number. This effect is quantitatively predicted by a quasi-steady and quasi-cylindrical analytical model. The model, combined with empirical data for the decay of axial swirl in pipe flows, predicts the observed influence of the distance between the vortex wave generator and the nozzle. The findings presented here contradict the hypothesis found in the literature, which presumes that sound production in the aforementioned experiment is due to the acceleration of vorticity waves through the nozzle.

Nomenclature

$A(x)$	=	cross-sectional surface at axial position x, m^2
A_{th}	=	cross-sectional surface in the throat, m^2
A_1	=	upstream pipe section cross-sectional surface area, m^2
A_2	=	downstream cross-sectional surface area, m^2
c	=	local sound speed, $m \cdot s^{-1}$
c_p	=	specific heat at constant pressure, $J \cdot kg^{-1} \cdot K^{-1}$
c_r	=	reservoir sound speed, $m \cdot s^{-1}$
c_{th}	=	sound speed at nozzle throat, $m \cdot s^{-1}$
c_v	=	specific heat at constant volume, $J \cdot kg^{-1} \cdot K^{-1}$
c_θ	=	sound speed in injection reservoir, $m \cdot s^{-1}$
c_2	=	sound speed in downstream section, $m \cdot s^{-1}$
c^*	=	critical sound speed, $m \cdot s^{-1}$
f_1	=	upstream quarter-wavelength oscillation frequency, Hz
f_2	=	downstream quarter-wavelength oscillation frequency, Hz
L_1	=	upstream pipe section length, m
M	=	Mach number
M_{th}	=	Mach number in the throat
M_2	=	Mach number in downstream section
$\dot{m}_{st}$	=	stationary mass flux, $kg \cdot s^{-1}$
$\dot{m}_{th}$	=	mass flux through throat, $kg \cdot s^{-1}$
$\dot{m}_\theta$	=	mass flux of tangential injection, $kg \cdot s^{-1}$
$\dot{m}_1$	=	mass flux in upstream section, $kg \cdot s^{-1}$
$\dot{m}^*$	=	critical quasi-one-dimensional isentropic irrotational mass flux, $kg \cdot s^{-1}$
p_{atm}	=	atmospheric pressure, Pa
p_r	=	reservoir pressure, Pa
p_θ	=	injection reservoir pressure, Pa
p_2'	=	downstream acoustic pressure pulse, Pa
R	=	specific gas constant, $J \cdot kg^{-1} \cdot K^{-1}$
R_{th}	=	nozzle throat radius, m
R_θ	=	injector outlet surface radius, m
R_1	=	upstream pipe section radius, m
Re_1	=	upstream Reynolds number
r	=	radial coordinate, m
S	=	swirl number
S_{th}	=	throat swirl number
S_0	=	stationary back ground swirl
S_1	=	upstream swirl number
$S_{1,VWG}$	=	swirl number at the injection point
T_r	=	reservoir temperature, K
T_{th}	=	temperature at nozzle throat, K
T^*	=	critical temperature, K
t	=	time, s
u_x	=	axial velocity, $m \cdot s^{-1}$
u_θ	=	azimuthal velocity due to tangential air injection, $m \cdot s^{-1}$
u_2	=	axial velocity in downstream section, $m \cdot s^{-1}$
u_2'	=	acoustic velocity fluctuation in downstream section, $m \cdot s^{-1}$
u^*	=	critical velocity, $m \cdot s^{-1}$
V_{set}	=	settling chamber volume, m^3
x	=	axial coordinate, m
β	=	exponential swirl-decay rate
γ	=	specific heat ratio; c_p/c_v
Δx	=	distance in the streamwise direction from the tangential injector, m
$\delta\dot{m}/m^*$	=	relative mass flux variation
$\delta\dot{m}_{st}/m^*$	=	quasi-steady relative mass flux reduction
μ	=	dynamic viscosity, $Pa \cdot s$
ρ	=	local density, $kg \cdot m^{-3}$
ρ_θ	=	injection air density, $kg \cdot m^{-3}$

Presented as Paper 2020-2532 at the AIAA Aviation 2020 Forum, June 15–19, 2020; received 6 April 2020; revision received 22 September 2020; accepted for publication 27 September 2020; published online 5 November 2020.

*DLR-DAAD Postdoctoral Fellow, Institute of Propulsion Technology, Engine Acoustics, Mueller-Breslau-Strasse 8. Member AIAA.
†Assistant Professor, Faculty of Aerospace Engineering, Kluyverweg 1.
‡Team Leader Combustion Acoustics, Institute of Propulsion Technology, Engine Acoustics, Mueller-Breslau-Strasse 8. Member AIAA.

ρ_1 = upstream density, kg · m^{-3}
ρ_2 = density in downstream section, kg · m^{-3}
ρ^* = critical density, kg · m^{-3}
τ_{set} = settling chamber pressure variation time scale, s

I. Introduction

A KEY source of noise in turbulent combustion is unsteady gas expansion, which produces what is known as direct-combustion noise [1–4]. However, significant levels of indirect-combustion noise can also be produced by flow inhomogeneities. These include patches of fluid with differing entropy arising from nonuniform combustion, discrete vortices arising from unsteady flow separation, and compositional inhomogeneities arising from incomplete mixing, dilution, and variations in gas composition [1–4]. When such inhomogeneities leave the combustion chamber through a nozzle, sound waves are generated: some of which travel back into the chamber while others radiate outward. The sound waves returning to the combustion chamber can produce new inhomogeneities, which can result in a feedback loop that destabilizes the combustion process. Waves radiated outward are also undesirable because they contribute to environmental noise. Indirect-combustion noise due to entropy patches it is referred to as "entropy noise" due to compositional inhomogeneities such as "compositional noise" and due to vortices as "vorticity noise" [1–3].

Of the three indirect-combustion types, entropy noise has been the most extensively studied [1,2] and has been experimentally observed in isolation [5]. Compositional noise has only received attention more recently [3,4]. Vorticity noise, on the other hand, has not been the focus of great research interest. Consequently, entropy noise and indirect-combustion noise are often taken to be synonymous [1]. Nonetheless, as Morgans and Duran [1] stated, "the term 'indirect combustion noise' refers to the noise generated by the acceleration of both entropy and vorticity waves. The acceleration of vorticity waves also generates sound". Dowling and Mahmoudi explained [2] "combustion also generates unsteady shear leading to vorticity perturbations, which also convect and generate pressure perturbations as they accelerate through the turbine nozzle guide vanes. . . . Acceleration of entropy and vorticity waves in the choked nozzle results in generation of pressure waves that propagate upstream . . . and downstream from the turbine stage as indirect combustion noise." Vorticity noise is known to play a major role in the establishment of self-sustained pressure pulsations in large solid rocket motors [6–16] and is believed to be a possible indirect-combustion noise source in aircraft engines and turbine combustors [1,2,17,18].

Kings and Bake [17] performed a series of unique experiments with the aim of advancing the fundamental understanding of vorticity noise. These experiments were performed using a modified version of the experimental setup used for earlier canonical entropy wave generator experiments [5]. A schematic of the setup is shown in Fig. 1. Specifically, the heating module in the entropy wave generator experimental setup was replaced by a vorticity wave generator (VWG) module, shown in Fig. 2. Since it is difficult to distinguish between entropy and vorticity noise in experiments involving combustion, these experiments were performed using a cold gas (i.e., without combustion) in an attempt to observe vorticity noise in isolation.

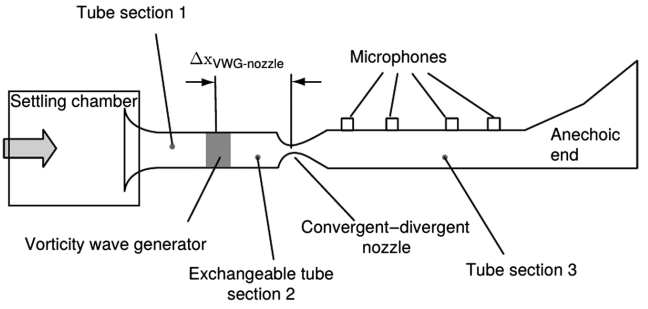

Fig. 1 Schematic of the vortex wave generator experimental setup. Figure taken from Ref. [17].

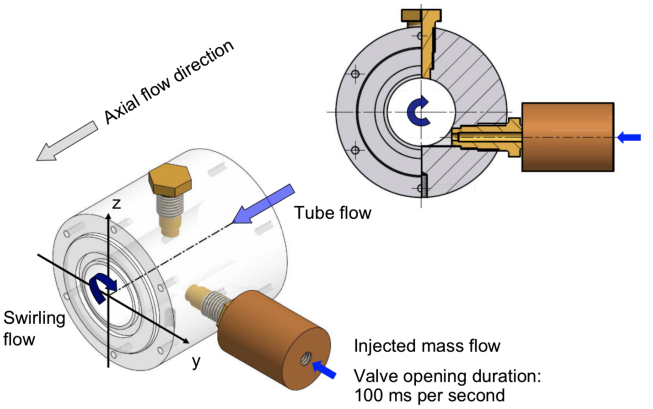

Fig. 2 The vorticity wave generator module (100 ms = 0.1 s).

Kings and Bake [17] hypothesized that the sound production in the experiments was due to acceleration of vorticity through the nozzle [17]. Indeed, in their conclusion, Kings and Bake [17] stated "The generation of vortex noise due to acceleration of artificial vorticity waves has been demonstrated in a model test rig." This assertion was likely inspired by Howe and Liu's [19] paper. However, it was not based on the actual application of Howe and Liu's [19] model. Howe and Liu [19] presented a low-Mach-number theory for the interaction of linear vorticity waves with a duct contraction [19]. The nozzle in Kings and Bake's experiment [17] was choked; i.e., the flow was transonic. Furthermore, in the set of experiments considered here, a strong swirl was suddenly introduced into a swirl-free initial choked nozzle flow state. This, as will be argued in this paper, induces an essentially nonlinear (in terms of swirl) aeroacoustic response of the system. Thus, although Howe and Liu's [19] paper is certainly interesting, the authors believe that the model is not applicable to the experiment reported in Ref. [17].

Kings [20,21] also obtained results with a different VWG module than the one used for experiments in Ref. [17]. In Ref. [20], Kings reported acoustic signals obtained with VWG1 and VWG2 modules, respectively. The VWG1 module is the same as was used for the results in Ref. [17] but with a single tangential-injection port as shown in Fig. 2. VWG2 was different; it had eight tangential-injection ports, four of which injected permanently, establishing a stationary background flow with swirl S_0. The other four injectors were used to perturb the stationary swirling background flow by periodic unsteady air injection. For the most part, the VWG2 experiments are not analyzed in the present paper. Kings [21] performed radial injection experiments too. The acoustic response obtained with radial injection was strikingly different than the ones obtained with tangential injection. Specifically, the downstream response obtained with radial injection had the opposite sign and was an order of magnitude lower in amplitude. Thus, tangential injection was essential for the strong acoustic response reported in Refs. [17,20].

Kings's Ph.D. thesis [20] reported hot-wire measurements of the velocity field performed upstream from the nozzle and downstream from the injection port in a measurement plane perpendicular to the streamwise direction. Unfortunately, these measurements do not include the flow in a 3 mm layer on the pipe wall, where a thin wall-bounded jet is expected. Another drawback of the hot-wire measurements is that these only measured absolute values of the velocity.

In the literature, no attempts at model-based analysis of Kings and Bake's [17] experiments, obtained with a VWG1 module, were found. In this paper, for the first time, such analysis is proposed.

For the VWG2 experiments, only one attempt at model-based analysis, by Ullrich et al. [18], was found in the literature. Ullrich et al. [18] did not model the response to the unsteady change in swirl δS due to periodic injection. Instead, a steady Reynolds-averaged Navier–Stokes solution for the flow resulting from constant injection through the four injection ports is used as a base flow for linearized Navier–Stokes simulations in the frequency domain. In the latter, vorticity waves were removed upstream of the nozzle using an analytical body-force term. While Ullrich et al.'s [18] approach is

interesting in its own right, it does not explicitly relate the experimentally observed sound production to the experimentally set driving parameters. In contrast to Ullrich et al.'s [18] numerical simulation-based approach, in the present paper, the authors have sought a highly simplified analytical model.

In Sec. II, the experiment is described in more detail. A discussion concerning the generated swirling flow is provided in Sec. III. A quasi-steady model for sound production due to interaction of the swirl component of the flow with the nozzle is presented and used for the analysis of the experimental results in Sec. IV.

II. Vorticity Wave Generator Experiment

In Sec. II.A, the experimental setup used by Kings and Bake [17] is described in detail. In Sec. II.B, Kings and Bake's [17] recorded signal is discussed.

A. Experimental Setup

In Fig. 1, a schematic sketch of the experimental setup is shown. The upstream part of the setup consisted of an upstream settling chamber (with a volume of 4.61) with a bell-mouth inlet to a tube section. The tube section had a 15 mm radius and 100 mm length (tube section 1 in Fig. 1). A single vorticity wave generator (VWG1) was connected to the downstream end of this tube section. The VWG1 was followed by a uniform exchangeable tube with a radius of 15 mm (section 2 in Fig. 1). Tube lengths of 50, 100, and 200 mm could be used, resulting in short, medium, and long configurations. After section 2 was a converging–diverging nozzle with a throat diameter of 7.5 mm and a surface contraction ratio of 1/16. Downstream from the nozzle was a uniform tube with a radius of 20 mm and a length of 1020 mm, referred to as the "microphone section." Four microphones (GRAS 40BP 1/4 in. externally polarized pressure microphones) were mounted flush in its walls. These were used to detect pressure waves generated by flow structure–nozzle interaction. An "anechoic" termination was connected to the microphone section by a flexible tube (radius of 20 mm and 980 mm length). (The termination was found to not be completely anechoic in numerical studies of Bake et al.'s entropy wave generatorexperiment [5,22,23]. Specifically, the termination is not anechoic at very low frequencies.) The effect of acoustic reflections from this termination (at low frequencies) is discussed in Sec. II.B.

A stationary nonswirling axial base flow was created by imposing a mass flow rate of 41 $\text{kg} \cdot \text{h}^{-1}$ in the settling chamber. At this mass flow rate, choked nozzle conditions were obtained with a reservoir pressure of $p_r = 1.114$ bar. This imposed an upstream nominal inlet Mach number of $M = 3.67 \times 10^{-2}$. The downstream section pressure was atmospheric with a Mach number of $M_2 = 2.2 \times 10^{-2}$.

Within VWG1, a small nozzle with an outlet radius of 1.5 mm was used to tangentially inject gas into the base flow. The injection was done using a fast-switching valve for the first 0.1 s of the 1 s experiment time. The opening and closing times of the valve were on the order of 2.5 ms (further details about the fast-switching valve can be found in Ref. [24]). For the experimental results analyzed in this text, the tangential-injection reservoir pressure p_θ was varied between 3 and 5 bar.

The mass injection rates reported by Kings and Bake [17,20,21] should actually have been determined using the reservoir pressure p_θ of the injection system. As is detailed in Appendix A, the initial tangential mass injection rate is estimated to be about 30 $\text{kg} \cdot \text{h}^{-1}$ for $p_\theta = 5$ bar. The flow meter had a response time on the order of 2 s, and was therefore inadequate to measure fast varying mass flows. Therefore, the authors use the reservoir pressure p_θ in the tangential-injection system to specify the flow conditions of the tangential-injection experiments.

In Fig. 2, one can see a closed radial injection port. As radial injection does not generate a swirling flow component, Kings used it to study "direct noise" caused by the radial injection of gas into a stationary choked flow [21]. Kings showed that when the nozzle is critical, most of the direct noise due to radial gas injection is reflected back upstream, while only a small part travels downstream through the sonic line. For radial injection with $p_\theta = 5$ bar into the same base flow as used for the tangential-injection experiments, Kings reported a positive pressure signal (measured with microphone 2) with an amplitude of approximately 10 Pa.

B. Recorded Acoustic Signal

The pressure signals due to tangential air injection reported by Kings and Bake [17] are shown in Figs. 3 and 4. The signals were recorded with the second microphone downstream from the nozzle throat, referred to as microphone 2. The distance between the nozzle throat and microphone 2 was 730 mm. In the plots, the pressure signal p_2' is shown as a function of time. As described in Ref. [17], the trigger signal to open and close the injection valve was given at the times of $t = 0.1$ s and $t = 0.2$ s, indicated in the figures with vertical dashed black lines.

The section 2 pipe lengths considered were 50 mm (short configuration, used for the blue line in Fig. 3), 100 mm (medium configuration, used for the red line in Fig. 3 and for the results shown in Fig. 4), and 200 mm (long configuration, used for the green line in Fig. 3). The signals in Fig. 4 were obtained using the medium configuration with six reservoir pressures of the tangential mass-injection system in the range 3 bar $< p_\theta <$ 5 bar (absolute).

Figure 3 shows the influence of a varied section 2 pipe length on the first part of the experimentally obtained signal. The beginning of the

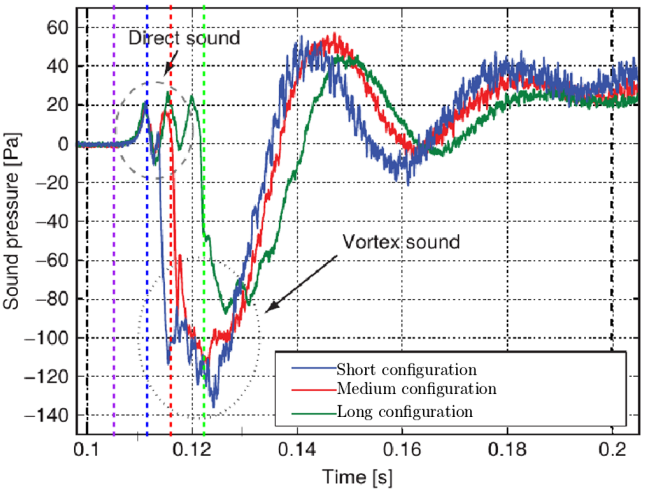

Fig. 3 Influence of section 2 length on acoustic signal, where blue, red, and green lines are for 50 mm (short), 100 mm (medium), and 200 mm (long) section lengths. Results obtained with for $p_\theta - p_{\text{atm}} = 4$ bar. Original figure from Ref. [17] and annotated.

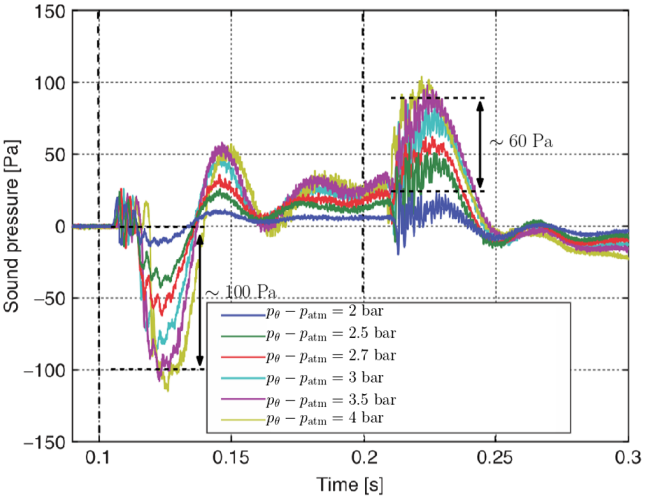

Fig. 4 Downstream recorded pressure signal due to swirl–nozzle interaction. Results obtained with the medium configuration. Annotated image; original taken from Ref. [17].

strong acoustic pressure peak induced by the entrance of the swirl into the nozzle (indicated by the blue, red, and green vertical lines in Fig. 3) occurs with a time delay relative to the beginning of the direct sound generated by the unsteady volume injection at 0.105 s (purple vertical dashed line). This time delay can be estimated as the convection time between the injection point and the nozzle inlet. For the three configurations, these distance were 85, 135, and 235 mm, respectively. The main flow velocity of 12.5 $\mathrm{m \cdot s^{-1}}$ ($M = 3.67 \times 10^{-2}$) led to convective delays of 6.8, 10.8, and 18.8 ms. The sound generated by vorticity noise should therefore begin at $t = 0.112$, 0.116, and 0.124 s, respectively. This agrees qualitatively with the experimental results shown in Fig. 3, confirming that the observed negative acoustic peak is due to the arrival of the vortex at the nozzle.

At $t \simeq 0.13$ s one observes a negative acoustic pressure peak difference of 40 Pa between the results obtained with the long configuration and those of the short configuration. This difference can be explained by swirl decay in the upstream tube and is expanded upon in Secs. III.B and IV.

For a reservoir pressure of 5 bar in the injection system, an oscillating signal with a frequency of 2×10^2 Hz is observed approximately 5 ms after the valve is opened. In the legend of Fig. 4, the pressure difference between the reservoir pressure in the injection system p_θ and the atmospheric pressure p_{atm} is indicated.

This first recorded signal is due to a quarter-wavelength oscillation caused by the abrupt start of tangential mass injection in the pipe section upstream of the nozzle throat (in Fig. 1: tube section 1, VWG1, and section 2). This signal is referred to as direct sound because it does not involve the interaction of the nozzle with the structure generated by tangential mass injection. Section 1, the VWG1 module, and section 2 have combined lengths of 0.220, 0.270, and 0.370 m for the short, medium, and long configurations, respectively. Assuming an end correction for the open side of the tube (at bell-mouth inlet) of 0.03 m, one can estimate the frequency of a quarter-wavelength oscillation in the upstream pipe sections. Using $f_1 = c/(4L_1)$, one estimates quarter-wavelength oscillation frequencies of 3.4×10^2, 2.8×10^2, and 2.1×10^2 Hz for the short, medium, and long configurations, respectively. Essentially, these correspond to what was experimentally observed. Specifically, using Fig. 3, one estimates for the short, medium, and long configurations' direct noise quarter-wavelength oscillation frequencies of 3.4×10^2, 2.6×10^2, and 2.2×10^2 Hz.

After this signal, there is a second lower-frequency (28 Hz) strongly damped acoustic pressure signal (Fig. 4). Initially, this has a strong negative peak related to a decrease of mass flux through the nozzle throat when the generated swirling flow structure enters the nozzle. The following 28 Hz oscillation corresponds to a strongly damped quarter-wavelength in the part of the experimental setup downstream from the nozzle throat. It is most pronounced for $p_\theta - p_{\mathrm{atm}} = 4$ bar. With an effective diffuser section length of $0.250/3$ m $\simeq 8 \times 10^{-2}$ m, a microphone section length of 1.02 m, and a flexible tube length of 0.98 m; and assuming the termination module to have an acoustic-effective length of 0.92 m, one estimates $f_2 \simeq 340\ \mathrm{m \cdot s^{-1}}/(4 \times 3.0\ \mathrm{m}) \simeq 28$ Hz. As will be explained in more detail in Sec. IV, the authors believe this signal is triggered by the decrease in mass flux through the nozzle caused by the presence of the swirl component in the nozzle throat. A more detailed discussion of the acoustic response of the downstream part of the system is provided in Refs. [5,23]. This includes data on measurements of the acoustic response of the downstream termination.

After a delay of approximately 5 ms following the electrical signal at 0.2 s driving the closing of the tangential mass injection valve, one again observes a 2.6×10^2 Hz quarter-wavelength oscillation of the upstream pipe section (with respect to the nozzle throat). Superimposed on this 2.6×10^2 Hz oscillation, one observes a strong oscillation at about 1 kHz. The 1 kHz is assumed to be due to a quarter-wavelength oscillation in the injection pipe, between the injection orifice and the closed fast valve (corresponding to an effective length of approximately 8 cm). The 2.6×10^2 Hz signal is observed as a modulation of the amplitude of the 1 kHz signal. This is followed by a superimposed strongly damped 28 Hz quarter-wavelength oscillation in the downstream part of the setup. This strongly damped oscillation has an initial positive peak. Its origin is the abrupt increase of mass flux through the nozzle as the swirl component leaves the nozzle. This sound production mechanism will be expanded on in Sec. IV.

It is interesting to note that there is some asymmetry between the initial negative pulse observed at 0.13 s, of approximately −100 Pa due to the entrance of the vortex in the nozzle, and the positive pulse at 0.23 s of approximately +60 Pa generated as the vortex leaves the nozzle (see Fig. 4 for $p_\theta - p_{\mathrm{atm}} = 4$ bar). Before the valve is opened, air in the pipe upstream from the valve including the tube section upstream from the Bronckhorst F-203AV linear resistance flow meter is at reservoir pressure (5 bar absolute). When the valve is opened, air situated in the tube connecting the valve to the flow meter is injected tangentially into the axial main flow initially at a rate of approximately 30 $\mathrm{kg \cdot h^{-1}}$. Because of the flow resistance of the meter, this lowers the pressure in the tube section between the valve and flow meter with respect to the reservoir pressure upstream from the flow meter. Thus, during the time the valve is opened, this pressure driving the tangential-injection mass flow rate decreases below p_θ. This leads to a decrease in swirl during the experiment, which could partially explain the observed asymmetry in the acoustic pressure signal between the opening and closing of the valve.

III. The Swirling Flow in the Experiment

A. Remarks Concerning the Flow due to Unsteady Mass Injection

Particle image velocimetry measurements reported in Refs. [17,21] and hot-wire measurements in Ref. [20] point to a thin wall-bounded jet swirling flow being due to tangential air injection in the experiments.

However, a precise description of the resulting swirling flow is currently not possible due to its complex nature. This was first indicated in figure 5.22(a) on page 101 in Ref. [20], where comparison is made between the absolute values of the axial velocity profiles $|u_x(r)|$, measured by means of a hot wire, in the pipe before injection and 0.05 s after the start of the injection. The central part of the flow ($r < 6$ mm) is most probably directed toward the (upstream) settling chamber. The external part (6 mm $< r <$ 15 mm) is likely directed toward the nozzle inlet. Using this assumption, one can verify that the volume flux does not change much between the initial flow before injection and 0.05 s after the start of injection.

That the volume flow remains almost constant is confirmed by the fact that the settling chamber time constant for a change in reservoir pressure is $\tau_{\mathrm{set}} = \rho_1 V_{\mathrm{set}}/\dot{m}_1 \simeq 0.7$ s. If one would assume that the flow is directed entirely downstream, the volume flow would have to almost double. However, the volume flow cannot change by a factor of two within 0.05 s. Hence, it is most likely that a reversed jet flow dominates the center of the pipe flow upstream from the nozzle.

As the hot-wire measurements could not be performed near the wall of the upstream tube (the measurements in Ref. [20] are only available for $r < 12$ mm), they only offer partial insight into the nature of the generated flow.

In the literature, one finds the following definition of swirl intensity [25–27]:

$$S = \frac{2\pi \int_0^{R_1} \rho u_x u_\theta r^2 \, \mathrm{d}r}{2\pi R_1 \int_0^{R_1} \rho u_x^2 r \, \mathrm{d}r} \tag{1}$$

The authors were unable to derive a simple equation relating the experimentally set parameters $\dot{m}_1$, R_1, $\dot{m}_\theta$, and R_θ to the swirl intensity as defined earlier in this paper. Part of $\dot{m}_\theta$ is likely directly deflected toward the settling chamber. This means that flow prediction can only be done by means of numerical simulations that take the presence of the settling chamber into account.

Moving forward, the authors make the following ansatz: the experimentally set swirl intensity is proportional to the tangentially injected mass flow rate $\dot{m}_\theta$. One knows that $\dot{m}_\theta$ depends linearly on the injection reservoir pressure p_θ (Appendix A). With that in mind, in Fig. 5, the authors have plotted the amplitude of the downstream measured pressure response $|p_{2'}|$ as a function of the relative injection absolute reservoir pressure squared p_θ^2. A linear fit (with a regression factor of 0.99) indicates that the downstream acoustic response $p_{2'}$ depends

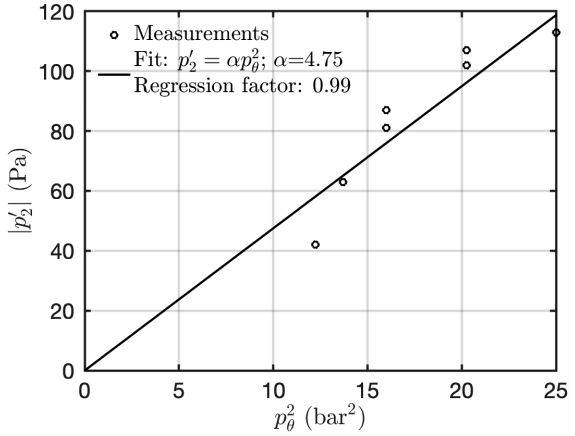

Fig. 5 Amplitude of downstream recorded acoustic response $|p_2'|$ as a function of the absolute injection reservoir pressure squared p_θ^2 for $p_\theta \geq 3.5$ bar.

quadratically on the injected mass flow rate $\dot{m}_\theta$ for $p_\theta \geq 3.5$ bar. This corresponds to what was reported in Ref. [20]. Thus, as anticipated, the downstream p_2' depends quadratically on the swirl intensity.

The authors extend their ansatz by assuming that, with respect to the unperturbed quasi-steady one-dimensional mass flow $\dot{m}^*$, the relative change in the mass flow rate ($\delta\dot{m}_{\text{st}}/\dot{m}^*$) due to the presence of a tangential flow component can be expressed as a function of the swirl intensity at the throat of S_{th} squared. This assumption is supported by data reported in figure 6 of Ref. [25], in which $\delta\dot{m}_{\text{st}}/\dot{m}^*$ for uniform ($n = 0$), solid body rotation ($n = 1$), and exponential tangential velocity profiles are shown. In figure 6 of Ref. [25], $\delta\dot{m}_{\text{st}}/\dot{m}^*$ as a function of S_{th}^2 for $n = 0$ and $n = 1$ are quite nearly identical. The relative difference between $n = 0$ and the exponential tangential velocity profile is about 20%. Thus, for sake of simplicity, to develop a model, the authors have assumed u_θ to be uniform. The authors then followed van Holten et al.'s [28] modeling approach (details in Appendix B), which yields

$$\frac{\delta\dot{m}_{\text{st}}}{m^*} = -\frac{9}{8}S_{\text{th}}^2 \tag{2}$$

This result is the same as reported for $n = 0$ in figure 6 of Ref. [25]. Expressed in terms of the swirl intensity at the nozzle inlet S_1, Eq. (2) becomes

$$\frac{\delta\dot{m}_{\text{st}}}{\dot{m}^*} = -\frac{9}{8}S_1^2\left(\frac{R_{\text{th}}}{R_1}\right)^2\left(\frac{2}{\gamma+1}\right)^{2/(\gamma-1)} \tag{3}$$

where R_{th} and γ are the radius at the throat and the heat capacity ratio, respectively. Equation (3) was derived from Eq. (2) by using the conservation of mass flow and impulse momentum, with the assumption of the preservation of the tangential flow profile.

B. Viscous Swirl Decay

Steenbergen and Voskamp [26] describe the decay of swirl in a pipe flow as a process caused by the transport of angular momentum to the pipe wall, viz., viscous action. The process was found to depend on the Reynolds number Re. The Reynolds number in the upstream pipe section of Kings and Bake's experiment [17,21] is estimated as follows:

$$Re_1 = \frac{\rho_1 u_x(2R_1)}{\mu} \simeq 2.7 \times 10^4$$

where μ is the dynamic viscosity of the flow.

Following Ref. [26], a simple relation for the ratio of swirl at distance Δx in the streamwise direction from the injection point $S_1(\Delta x)$ and the swirl at the injection point $S_{1,\text{VWG}}$ (i.e., the swirl reduction factor) is proposed:

$$\frac{S_1(\Delta x)}{S_{1,\text{VWG}}} = \exp\left(-\beta\frac{\Delta x}{2R_1}\right) \tag{4}$$

where the exponential swirl-decay rate β is in the range $0.03 \leq \beta \leq 0.04$ for the preceding Reynolds number.

Thus, for a 50 mm pipe length of section 2, at the nozzle inlet ($\Delta x = 85$ mm), one finds a swirl reduction factor with respect to $S_{1,\text{VWG}}$ of 0.92. For a section 2 length of 200 mm, one finds a swirl reduction factor with respect to $S_{1,\text{VWG}}$ of 0.79 [i.e., addition of a 150 mm pipe to section 2 causes a swirl reduction of 0.86 relative to the initial (shorter) configuration]. The effect of swirl decay will be used in Sec. IV to explain the difference in results between the short, medium, and long configurations, shown in Fig. 3.

IV. Swirl–Nozzle Interaction Sound Production Model

The variation in mass flow rate ($\delta\dot{m}/\dot{m}^*$) caused by the swirl component entering and exiting the nozzle will induce expansion and compression acoustic waves downstream. If one neglects the influence of the weak normal shock in the divergent part of the nozzle, the effect of the normal vortex component (normal to the duct axis), the time dependence of the upstream settling chamber pressure, and the influence of entropy inhomogeneity associated with the generation of a swirling flow structure; and assumes a low-Mach-number flow in the downstream pipe of uniform cross-section A_2, one has

$$\frac{u_2'}{u_2} = \frac{\delta\dot{m}}{\dot{m}^*} \tag{5}$$

where

$$\frac{\delta\dot{m}}{\dot{m}^*} = \begin{cases} +\dfrac{\delta\dot{m}_{\text{st}}}{\dot{m}^*} & \text{after the valve is opened} \\ -\dfrac{\delta\dot{m}_{\text{st}}}{\dot{m}^*} & \text{after the valve is closed} \end{cases} \tag{6}$$

One can then estimate the acoustic pressure pulse p_2' generated in the section downstream from the nozzle using

$$p_2' \simeq \rho_2 c_2 u_2' \tag{7}$$

This is the pressure pulse amplitude one would measure in an infinitely long downstream tube (anechoic termination). The acoustic model could be used to estimate S_1 from p_2'. However, this is not explored further in the present paper.

Had one had a straightforward expression for $S_{1,\text{VWG}}$, one would have been able to estimate S_1 and then determine u_2' from Eq. (5): the result of which would be used with Eq. (7) to calculate p_2'. However, as explained in Sec. III.A, no straightforward method for estimating $S_{1,\text{VWG}}$ has been found by the authors.

Thus, an alternative means of validation is pursued. Consider Fig. 3, in which the influence of the section 2 length variation on the acoustic signal is shown. One observes, for example, a decrease of approximately 40 Pa between the short configuration (blue line) and the long configuration (green line) of section 2. By virtue of Eqs. (3), (5), and (7), one has

$$p_2' \propto S_1^2 \tag{8}$$

The effect of swirl decay, discussed in Sec. III.B, will be used to estimate the pressure difference $\Delta p_2'$ between two configurations of the setup. To estimate $\Delta p_2'$, the following is used:

$$\Delta p_2' \simeq \left(1 - \exp\left(-\beta\frac{\Delta L_1}{R_1}\right)\right) \times 120 \text{ Pa} \tag{9}$$

where ΔL_1 is the difference in upstream pipe length between two configuration, and 120 Pa is taken to be the maximum amplitude of the short configuration. Using the preceding expression, one finds

$$\Delta p_2' \simeq \begin{cases} 35 \pm 4 \text{ Pa between long and short,} \\ 13 \pm 2 \text{ Pa between medium and short} \end{cases} \quad (10)$$

which is in satisfactory agreement with what one sees in Fig. 3.

V. Conclusions

In the experiments analyzed in this paper, the most important contribution to the recorded acoustic signal is due to the passage of the swirl component of the upstream-generated structure. As it transits through the nozzle, it temporarily reduces the mass flux through the nozzle throat. A quasi-steady model of this effect, which includes a model for viscous swirl decay to predict the influence of the distance between the injection point and the choked nozzle inlet, was used to explain the difference between the short, medium, and long upstream channel configurations in the experiments. The model predicts an essentially quadratic swirl number dependence of the generated sound amplitude. These findings contradict the hypothesis found in the literature, which presumes that sound production in the aforementioned experiment is due to the acceleration of vorticity waves through the nozzle.

Appendix A: Estimated Tangential Mass Injection

In the pipe upstream from the choked nozzle, air was tangentially injected with a mass flow rate $\dot{m}_\theta$. Before tangential injection was initiated, the reservoir pressure upstream was $p_r = 1.114$ bar. Tangential injection was done through an injection port of radius of $R_\theta = 1.5$ mm. There was a flow meter between the injection valve and reservoir, which implies flow resistance. Initially, as the valve was opened, the pipe between the valve and flow meter acted as a reservoir at p_θ bar. Given that $p_\theta \gg p_r$, the tangential-injection port will be choked.

Assuming a frictionless steady flow, one can estimate the initial value of $\dot{m}_\theta$ using the compressible Bernoulli equation for a perfect gas [29]:

$$\dot{m}_\theta = \rho_\theta c_\theta \left(\frac{2}{\gamma+1}\right)^{(\gamma+1)/2(\gamma-1)} \pi R_\theta^2 \quad (A1)$$

For $p_\theta = 5$ bar, $\rho_\theta = 6 \text{ kg} \cdot \text{m}^{-3}$ is the reservoir density, $c_\theta = 340 \text{ m} \cdot \text{s}^{-1}$ is the speed of sound at reservoir temperature, and $\gamma = 1.4$ is the heat capacity ratio of air; and one finds $m_\theta = 30 \text{ kg} \cdot \text{h}^{-1}$.

Appendix B: Response of a Choked Nozzle to a Swirl Fluctuation

In this appendix, for given fixed reservoir conditions of pressure p_r and temperature T_r, an analytical model for the influence of the swirl component on the steady mass flow through a choked nozzle is presented. The approach described by van Holten et al. [28] is followed.

The circular cross section of the nozzle at axial position x is denoted $A(x)$. The nozzle throat corresponding to the minimum of cross section ($\mathrm{d}A/\mathrm{d}x = 0$) is A_{th}. The hypothetical quasi-one-dimensional isentropic irrotational mass flux $\dot{m}^*$ through a choked nozzle is given by

$$\dot{m}^* = \rho^* u^* A_{\text{th}} \quad (B1)$$

Here, the critical velocity u^* is equal to the critical speed of sound c^*. For an isentropic flow of an ideal gas with a constant specific heat ratio of $\gamma = c_p/c_v$ (c_p and c_v at constant pressure and volume, respectively), one thus has

$$u^* = c^* = \sqrt{\gamma R T^*} \quad (B2)$$

where $R = c_p - c_v$ is the specific ideal gas constant, and T^* is the critical temperature. T^* is related to the reservoir temperature T_r through Bernoulli's equation [29,30] as follows:

$$T^* = \frac{2}{\gamma+1} T_r \quad (B3)$$

Due to the axial rotation of the flow, the mass flux through the nozzle will be lower than $\dot{m}^*$. To account for this, it is assumed that entropy production during the generation of the swirl component is negligible. Furthermore, it is assumed that the total enthalpy of the flow remains constant and equal to the reservoir enthalpy. It is also assumed that the flow can be described as quasi one-dimensional, neglecting the nonuniformity induced by the change in cross section. For simplicity, it is assumed that the tangential velocity u_θ is uniform in each cross section. This approximation will be referred to as the "quasi-cylindrical" flow approximation here. In the quasi-cylindrical flow approximation, the local Mach number M at a specific point in the flow is related to the local axial velocity u_x and local tangential velocity u_θ through the definition

$$M^2 = \frac{u_x^2 + u_\theta^2}{c^2} \quad (B4)$$

The local speed of sound c is related to the reservoir value c_r through Bernoulli's equation as follows:

$$c_r^2 = c^2 + \frac{\gamma-1}{2}(u_x^2 + u_\theta^2) \quad (B5)$$

Substitution of Eq. (B5) into Eq. (B4) yields

$$M^2 = \frac{u_x^2 + u_\theta^2}{c_r^2 - [(\gamma-1)/2](u_x^2 + u_\theta^2)} \quad (B6)$$

This corresponds to van Holten et al.'s [28] model and Gany et al.'s model (for $n = 0$) [25].

These equations are complemented by the integral-mass-conservation law for the stationary mass flux $\dot{m}_{\text{st}}$

$$\dot{m}_{\text{st}} = \rho u_x A = \text{constant} \quad (B7)$$

or in differential form,

$$\frac{1}{\dot{m}_{\text{st}}}\frac{\mathrm{d}\dot{m}_{\text{st}}}{\mathrm{d}x} = \frac{1}{\rho}\frac{\mathrm{d}\rho}{\mathrm{d}x} + \frac{1}{u_x}\frac{\mathrm{d}u_x}{\mathrm{d}x} + \frac{1}{A}\frac{\mathrm{d}A}{\mathrm{d}x} = 0 \quad (B8)$$

From axial conservation of angular momentum, for a circular cross section, one has

$$\dot{m}_{\text{st}} u_\theta \sqrt{\frac{A}{\pi}} = \text{constant} \quad (B9)$$

or in differential form,

$$\frac{1}{\dot{m}_{\text{st}}}\frac{\mathrm{d}\dot{m}_{\text{st}}}{\mathrm{d}x} + \frac{1}{u_\theta}\frac{\mathrm{d}u_\theta}{\mathrm{d}x} + \frac{1}{2A}\frac{\mathrm{d}A}{\mathrm{d}x} = \frac{1}{u_\theta}\frac{\mathrm{d}u_\theta}{\mathrm{d}x} + \frac{1}{2A}\frac{\mathrm{d}A}{\mathrm{d}x} = 0 \quad (B10)$$

At the throat of the nozzle, where $(\mathrm{d}A/\mathrm{d}x)_{\text{th}} = 0$, using Eq. (B10), one finds that

$$\left(\frac{\mathrm{d}u_\theta}{\mathrm{d}x}\right)_{\text{th}} = 0 \quad (B11)$$

Mass conservation at the throat can then be written as

$$-\frac{1}{A}\frac{\mathrm{d}A}{\mathrm{d}x} = \frac{1}{\rho}\frac{\mathrm{d}\rho}{\mathrm{d}x} + \frac{1}{u_x}\frac{\mathrm{d}u_x}{\mathrm{d}x} = 0 \quad (B12)$$

or, noting that for steady isentropic flow $(1/\rho)\mathrm{d}\rho/\mathrm{d}x$ is a function of M^2 and Eq. (B11),

$$\frac{1}{\rho}\frac{\mathrm{d}\rho}{\mathrm{d}M^2}\left(\frac{\partial M^2}{\partial u_x}\frac{\mathrm{d}u_x}{\mathrm{d}x}+\frac{\partial M^2}{\partial u_\theta}\frac{\mathrm{d}u_\theta}{\mathrm{d}x}\right)+\frac{1}{u_x}\frac{\mathrm{d}u_x}{\mathrm{d}x}=0$$
$$\frac{1}{\rho}\frac{\mathrm{d}\rho}{\mathrm{d}M^2}\left(\frac{\partial M^2}{\partial u_x}\frac{\mathrm{d}u_x}{\mathrm{d}x}\right)+\frac{1}{u_x}\frac{\mathrm{d}u_x}{\mathrm{d}x}=0 \tag{B13}$$

where [by virtue of Eq. (B6)]

$$\frac{\partial M^2}{\partial u_x}=2\frac{u_x.c_r^2}{c^4} \tag{B14}$$

As the flow is assumed isentropic and the gas ideal, one finds

$$\frac{1}{\rho}\frac{\mathrm{d}\rho}{\mathrm{d}M^2}=-\frac{1}{2}\left(\frac{c}{c_r}\right)^2 \tag{B15}$$

Substitution of Eqs. (B14) and (B15) into Eq. (B13), because for a choked nozzle $(\mathrm{d}u_x/\mathrm{d}x)_{\mathrm{th}}\neq 0$, yields

$$(u_x)_{\mathrm{th}}=c_{\mathrm{th}} \tag{B16}$$

Consequently, the Mach number at the throat is

$$M_{\mathrm{th}}^2=1+\frac{(u_\theta)_{\mathrm{th}}^2}{c_{\mathrm{th}}^2} \tag{B17}$$

Using this and Eq. (B16), the stationary mass flux of $\dot{m}_{\mathrm{st}}=\dot{m}_{\mathrm{th}}$ (by conservation of mass) can be calculated for an isentropic flow using

$$\dot{m}_{\mathrm{st}}=\frac{\rho_{\mathrm{th}}c_{\mathrm{th}}}{\rho^*c^*}\rho^*c^*A_{\mathrm{th}} \tag{B18}$$

Assuming an isentropic flow of a perfect gas implies

$$\dot{m}_{\mathrm{st}}=\left(\frac{T_{\mathrm{th}}}{T^*}\right)^{(\gamma+1)/2(\gamma-1)}\dot{m}^* \tag{B19}$$

Using Bernoulli's principle for compressible flow and Eq. (B17), one finds

$$\frac{T_{\mathrm{th}}}{T^*}=\frac{(\gamma+1)/2}{1+[(\gamma-1)/2]M_{\mathrm{th}}^2}$$
$$=\frac{1}{1+[(\gamma-1)/(\gamma+1)]((u_\theta)_{\mathrm{th}}/c_{\mathrm{th}})^2} \tag{B20}$$

With a first-order Taylor expansion for $((u_\theta)_{\mathrm{th}}/c_{\mathrm{th}})^2\ll 1$, one obtains

$$\dot{m}_{\mathrm{st}}\simeq\left(1-\frac{1}{2}\left(\frac{(u_\theta)_{\mathrm{th}}}{c_{\mathrm{th}}}\right)^2\right)\dot{m}^* \tag{B21}$$

Using Eq. (B21), one can find an approximation for the quasi-steady relative mass flux reduction $(\dot{m}_{\mathrm{st}}-\dot{m}^*)/\dot{m}^*\equiv\delta\dot{m}_{\mathrm{st}}/\dot{m}^*$:

$$\frac{\delta\dot{m}_{\mathrm{st}}}{\dot{m}^*}\simeq-\frac{1}{2}\left(\frac{(u_\theta)_{\mathrm{th}}}{c_{\mathrm{th}}}\right)^2 \tag{B22}$$

Assuming a uniform tangential velocity u_θ, uniform axial velocity u_x, and uniform density ρ, the swirl number [Eq. (1)] becomes

$$S=\frac{2u_\theta}{3u_x} \tag{B23}$$

Equation (B22) becomes

$$\frac{\delta\dot{m}_{\mathrm{st}}}{\dot{m}^*}\simeq-\frac{9}{8}S_{\mathrm{th}}^2 \tag{B24}$$

In the upstream section with cross-sectional surface A_1, one finds, in terms of $(u_\theta)_1$ at A_1, using the conservation of angular momentum, assuming $M_1\ll 1$ and performing some algebra, Eq. (B24) becomes

$$\frac{\delta\dot{m}_{\mathrm{st}}}{\dot{m}^*}=-\frac{9}{8}S_1^2\frac{A_{\mathrm{th}}}{A_1}\left(\frac{2}{\gamma+1}\right)^{2/(\gamma-1)} \tag{B25}$$

Acknowledgment

This work was carried out while Lionel Hirschberg was the beneficiary of a Deutsches Zentrum für Luft- und Raumfahrt–Deutscher Akademischer Austauschdienst postdoctoral fellowship (no. 57424730).

References

[1] Morgans, A. S., and Duran, I., "Entropy Noise: A Review of Theory, Progress and Challenges," *International Journal of Spray and Combustion Dynamics*, Vol. 8, No. 4, 2016, pp. 285–298. https://doi.org/10.1177/1756827716651791

[2] Dowling, A. P., and Mahmoudi, Y., "Combustion Noise," *Proceedings of the Combustion Institute*, Vol. 35, No. 1, 2015, pp. 65–100. https://doi.org/10.1016/j.proci.2014.08.016

[3] Margi, L., O'Brien, F., and Ihme, M., "Compositional Inhomogeneities as a Source of Indirect Combustion Noise," *Journal of Fluid Mechanics*, Vol. 799, July 2016, Paper R4. https://doi.org/10.1017/jfm.2016.397

[4] Ihme, M., "Combustion and Engine-Core Noise," *Annual Review of Fluid Mechanics*, Vol. 49, 2017, pp. 277–310. https://doi.org/10.1146/annurev-fluid-122414-034542

[5] Bake, F., Richter, C., Mühlbauer, B., Kings, N., Röhle, I., Thiele, F., and Noll, B., "The Entropy Wave Generator (EWG): A Reference Case on Entropy Noise," *Journal of Sound and Vibration*, Vol. 326, Nos. 3–5, 2009, pp. 574–598. https://doi.org/10.1016/j.jsv.2009.05.018

[6] Dotson, K. W., Koshigoe, S., and Pace, K. K., "Vortex Shedding in a Large Solid Rocket Motor Without Inhibitors at the Segmented Interfaces," *Journal of Propulsion and Power*, Vol. 13, No. 2, 1997, pp. 197–206. https://doi.org/10.2514/2.5170

[7] Anthoine, J., "Experimental and Numerical Study of Aeroacoustic Phenomena in Large Solid Propellant Boosters, with Application to the Ariane 5 Solid Rocket Motor," Ph.D. Thesis, Free Univ. of Brussels, Brussels, Belgium, 2000.

[8] Hulshoff, S. J., Hirschberg, A., and Hofmans, G. C. J., "Sound Production of Vortex Nozzle Interactions," *Journal of Fluid Mechanics*, Vol. 439, July 2001, pp. 335–352. https://doi.org/10.1017/S0022112001004554

[9] Anthoine, J., Buchlin, J.-M., and Hirschberg, A., "Effect of Nozzle Cavity on Resonance in Large SRM: Theoretical Modeling," *Journal of Propulsion and Power*, Vol. 18, No. 2, 2002, pp. 304–311. https://doi.org/10.2514/2.5935

[10] Fabignon, Y., Dupays, J., Avalon, G., Vuillot, F., Lupoglazoff, N., Casalis, G., and Prévost, M., "Instabilities and Pressure Oscillations in Solid Rocket Motors," *Aerospace Science and Technology*, Vol. 7, No. 3, 2003, pp. 191–200. https://doi.org/10.1016/S1270-9638(02)01194-X

[11] Gallier, S., Prevost, M., and Hijlkema, J., "Effects of Cavity on Thrust Oscillations in Subscale Solid Rocket Motors," *45th AIAA/ASME/ASEE Joint Propulsion Conference and Exhibit*, AIAA Paper 2009-5253, Aug. 2009. https://doi.org/10.2514/6.2009-5253

[12] Hirschberg, L., Hulshoff, S. J., Collinet, J., Schram, C., and Schuller, T., "Vortex Nozzle Interaction in Solid Rocket Motors: A Scaling Law for Upstream Acoustic Response," *Journal of the Acoustical Society of America*, Vol. 144, No. 1, 2018, pp. EL46–EL51. https://doi.org/10.1121/1.5046441

[13] Hirschberg, L., Schuller, T., Collinet, J., Schram, C., and Hirschberg, A., "Analytical Model for the Prediction of Pulsations in a Cold-Gas Scale-Model of a Solid Rocket Motor," *Journal of Sound and Vibration*, Vol. 19, April 2018, pp. 445–368. https://doi.org/10.1016/j.jsv.2018.01.025

[14] Hirschberg, L., "Low Order Modeling of Vortex Driven Self-Sustained Pressure Pulsations in Solid Rocket Motors," Ph.D. Thesis, Univ. of Paris-Saclay, Gif-sur-Yvette, France, 2019.

[15] Hirschberg, L., Hulshoff, S. J., Collinet, J., Schram, C., and Schuller, T., "Influence of Nozzle Cavity on Indirect Vortex- and Entropy-Sound Production," *AIAA Journal*, Vol. 57, No. 7, March 2019, pp. 3100–3103. https://doi.org/10.2514/1.J058138

[16] Hirschberg, L., and Hulshoff, S. J., "Lumped-Element Model for Vortex–Nozzle Interaction in Solid Rocket Motors," *AIAA Journal*, Vol. 58, No. 7, May 2020, pp. 3241–3244. https://doi.org/10.2514/1.J058673

[17] Kings, N., and Bake, F., "Indirect Combustion Noise: Noise Generation by Accelerated Vorticity in a Nozzle Flow," *International Journal of Spray and Combustion Dynamics*, Vol. 2, No. 3, 2010, pp. 253–266. https://doi.org/10.1260/1756-8277.2.3.253

[18] Ullrich, W. C., Bake, F., Kings, N., and Sattelmayer, T., "Numerical Investigations of Indirect Noise Generation by Accelerated Vorticity," *21st AIAA/CEAS Aeroacoustics Conference*, AIAA Paper 2015-2382, June 2015. https://doi.org/10.2514/6.2015-2382

[19] Howe, M. S., and Liu, J. T. C., "The Generation of Sound by Vorticity Waves in Swirling Duct Flows," *Journal of Fluid Mechanics*, Vol. 81, No. 2, June 1977, pp. 369–383. https://doi.org/10.1017/S0022112077002109

[20] Kings, N., "Indirect Combustion Noise: Experimental Investigation of the Vortex Sound Generation in Nozzle Flows," Ph.D. Thesis, Technical Univ. of Berlin, Berlin, Germany, 2015.

[21] Kings, N., "Schallentstehung Durch Beschleunigte Wirbelstärke in Einer Düsenströmung," Diploma Thesis, Faculty V—Mechanical Engineering and Transport Systems, Diplomarbeit, Technical Univ. of Berlin, Berlin, Germany, 2009.

[22] Müllbauer, B., Noll, B., and Aigner, M., "Numerical Investigation of Entropy Noise and Its Acoustic Sources in Aero-Engines," ASME Paper GT2008-50321, New York, June 2008.

[23] Leyko, M., Moreau, S., Nicoud, F., and Poinsot, T., "Numerical and Analytical Modelling of Entropy Noise in a Supersonic Nozzle with a Shock," *Journal of Sound and Vibration*, Vol. 330, No. 16, Aug. 2011, pp. 3944–3958. https://doi.org/10.1016/j.jsv.2011.01.025

[24] Neuhaus, D., and Röhle, I., "Schnellschaltende Ventile für Anwendungen in der Luft und Raumfahrt," Deutscher Luft- und Raumfahrtkongress Paper DGLR-2006-098, Braunschweig, Nov. 2006, http://www.dglr.de/veranstaltungen/archiv.

[25] Gany, A., Mor, M., and Goldman, C., "Analysis and Characteristics of Choked Swirling Nozzle Flows," *AIAA Journal*, Vol. 43, No. 10, Oct. 2005, pp. 2177–2181. https://doi.org/10.2514/1.16887

[26] Steenbergen, W., and Voskamp, J., "The Rate of Decay of Swirl in Turbulent Pipe Flow," *Flow Measurement and Instrumentation*, Vol. 9, No. 2, June 1998, pp. 67–78. https://doi.org/10.1016/S0955-5986(98)00016-8

[27] Dutton, J. C., "Swirling Supersonic Flow," *Journal of Propulsion and Power*, Vol. 3, No. 4, July 1987, pp. 342–349. https://doi.org/10.2514/3.22996

[28] van Holten, T., Heiligers, M., and Jaeken, A., "Choking Phenomena in a Vortex Flow Passing a Laval Tube: An Analytical Treatment," *Journal of Fluids Engineering*, Vol. 131, No. 041201, April 2009, pp. 1–7. https://doi.org/10.1115/1.3089532

[29] Thompson, P. A., *Compressible-Fluid Dynamics*, McGraw–Hill, New York, 1972.

[30] Shapiro, A. H., *The Dynamics and Thermodynamics of Compressible Fluid Flow*, 1st ed., Vols. 1–2, Ronald, New York, 1953.

C. Bailly
Associate Editor